Available online at www.sciencedirect.com

ScienceDirect

Geochimica et Cosmochimica Acta 177 (2016) 94–104

Geochimica et Cosmochimica Acta

www.elsevier.com/locate/gca

Fe–O stable isotope pairs elucidate a high-temperature origin of Chilean iron oxide-apatite deposits

Laura D. Bilenker [a,*], Adam C. Simon [a], Martin Reich [b], Craig C. Lundstrom [c], Norbert Gajos [c], Ilya Bindeman [d], Fernando Barra [b], Rodrigo Munizaga [e]

[a] Department of Earth and Environmental Sciences, University of Michigan, 1100 North University Ave, Ann Arbor, MI, USA
[b] Department of Geology and Andean Geothermal Center of Excellence (CEGA), Universidad de Chile, Plaza Ercilla 803, Santiago, Chile
[c] Department of Geology, University of Illinois, 605 E. Springfield Ave., Champaign, IL, USA
[d] Department of Geological Sciences, University of Oregon, 1275 E 13[th] Ave., Eugene, OR, USA
[e] Compañia Minera del Pacífico, Brasil N 1050, Vallenar Región de Atacama, Chile

Received 4 September 2015; accepted in revised form 17 January 2016; available online 23 January 2016

Abstract

Iron oxide–apatite (IOA) ore deposits occur globally and can host millions to billions of tons of Fe in addition to economic reserves of other metals such as rare earth elements, which are critical for the expected growth of technology and renewable energy resources. In this study, we pair the stable Fe and O isotope compositions of magnetite samples from several IOA deposits to constrain the source reservoir of these elements in IOAs. Since magnetite constitutes up to 90 modal% of many IOAs, identifying the source of Fe and O within the magnetite may elucidate high-temperature and/or lower-temperature processes responsible for their formation. Here, we focus on the world-class Los Colorados IOA in the Chilean iron belt (CIB), and present data for magnetite from other Fe oxide deposits in the CIB (El Laco, Mariela). We also report Fe and O isotopic values for other IOA deposits, including Mineville, New York (USA) and the type locale, Kiruna (Sweden). The ranges of Fe isotopic composition (δ^{56}Fe, ^{56}Fe/^{54}Fe relative to IRMM-14) of magnetite from the Chilean deposits are: Los Colorados, δ^{56}Fe ($\pm 2\sigma$) = 0.08 ± 0.03‰ to 0.24 ± 0.08‰; El Laco, δ^{56}Fe = 0.20 ± 0.03‰ to 0.53 ± 0.03‰; Mariela, δ^{56}Fe = 0.13 ± 0.03‰. The O isotopic composition (δ^{18}O, ^{18}O/^{16}O relative to VSMOW) of the same Chilean magnetite samples are: Los Colorados, δ^{18}O ($\pm 2\sigma$) = 1.92 ± 0.08‰ to 3.17 ± 0.03‰; El Laco, δ^{18}O = 4.00 ± 0.10‰ to 4.34 ± 0.10‰; Mariela, δ^{18}O = (1.48 ± 0.04‰). The δ^{18}O and δ^{56}Fe values for Kiruna magnetite yield an average of 1.76 ± 0.25‰ and 0.16 ± 0.07‰, respectively. The Fe and O isotope data from the Chilean IOAs fit unequivocally within the range of magnetite formed by high-temperature magmatic or magmatic–hydrothermal processes (i.e., δ^{56}Fe 0.06–0.49‰ and δ^{18}O = 1.0–4.5‰), consistent with a high-temperature origin for Chilean IOA deposits. Additionally, minimum formation temperatures calculated by using the measured Δ^{18}O values of coexisting Los Colorados magnetite and actinolite separates (630 °C) as well as Fe numbers of actinolite grains (610–820 °C) are consistent with this interpretation. We also present Fe isotope data from magmatic magnetite of the Bushveld Complex, South Africa, where δ^{56}Fe ranges from 0.28 ± 0.04‰ to 0.86 ± 0.07‰. Based on these data and comparison to published Fe and O stable isotope values of igneous magnetite, we propose extending the magmatic/high-temperature δ^{56}Fe range to 0.86‰. Considering that the Chilean IOAs and Kiruna deposit are representative of IOA deposits worldwide, the Fe and O stable isotope data indicate that IOAs are formed by high-temperature (magmatic) processes.

* Corresponding author.
E-mail address: bilenker@umich.edu (L.D. Bilenker).

http://dx.doi.org/10.1016/j.gca.2016.01.009
0016-7037/

1. INTRODUCTION

The 600 km-long Chilean iron belt (CIB) in Northern Chile (25–31°S) hosts numerous Mesozoic Fe-rich ore deposits, many of which are characterized as iron oxide–apatite (IOA) or iron oxide–copper–gold (IOCG) deposits (e.g., Nyström and Henriquez, 1994; Oyarzún et al., 2003; Groves et al., 2010). The origin and classification of these types of deposits is widely debated, and working hypotheses include: (1) meteoric fluids (e.g., basinal brines) and hydrothermal replacement (e.g., Paràk, 1975, 1984; Barton and Johnson, 1996; Sillitoe and Burrows, 2002); (2) magmatic–hydrothermal fluids (e.g., Lundberg and Smellie, 1979; Pollard, 2006; Nyström et al., 2008; Richards and Mumin, 2013; Jonsson et al., 2013; Knipping et al., 2015a,b); and (3) immiscible Fe-rich and Si-rich melts (e.g., Kolker, 1982; Nyström and Henriquez, 1994; Naslund et al., 2002). A genetic connection between IOA and IOCG deposits has been proposed, wherein IOA deposits may represent the basal portion of IOCG systems (Naslund et al., 2002; Sillitoe, 2003). Iron oxide–apatite and IOCG deposits occur globally and individually host millions to billions of tons of their namesake metals and in some deposits economic reserves of uranium, rare earth elements (REEs), phosphorous, cobalt, silver, and/or titanium (Hitzman et al., 1992; Sillitoe, 2003; Groves et al., 2010; Richards and Mumin, 2013; Barton, 2014). Therefore, elucidating the source(s) of metals and the process(es) by which the deposits form is important for improving exploration strategies.

In this contribution, we pair non-traditional stable isotope data ($^{56}Fe/^{54}Fe$) with isotopic values from a stable isotope system ($^{18}O/^{16}O$) that has been well calibrated for deciphering the source of oxygen in rocks and minerals (Taylor, 1967; Hedenquist and Lowenstern, 1994; Bindeman, 2008) to fingerprint the source reservoir of Fe and O in magnetite in the world-class Los Colorados IOA deposit in Northern Chile. Los Colorados is one of the largest IOA deposits in the CIB and is representative of the nearly 50 IOAs in the region as well as those that exist globally. We also report Fe and O isotope ratio data for magnetite from several other deposits in the CIB, as well as the namesake Kiruna IOA deposit in Sweden. Magnetite can comprise >90 modal% of these deposits, and the Fe and O isotopic compositions of magnetite have been shown to be more resistant to secondary alteration than O and H isotopes in other mineral phases (Nyström et al., 2008; Jonsson et al., 2013; Weis, 2013). Further, we use O isotope values of actinolite-magnetite pairs from unaltered Los Colorados samples to calculate minimum formation temperatures (cf. Bindeman, 2008), and use the Fe/Mg ratio of the actinolite grains to provide further constraints on the origin of actinolite.

2. GEOLOGICAL SETTING

The Cretaceous Los Colorados deposit has been characterized as an IOA or Kiruna-type (“magnetite-apatite”) or simply “iron” deposit (e.g., Mathur et al., 2002; Oyarzún et al., 2003; Chen et al., 2013). It is the site of an active Fe mine ~35 km north of Vallenar, Chile within the Atacama Fault System (AFS) (Fig. 1) and contains ~350 Mt of Fe in two sub-parallel, sub-vertical magnetite-rich (up to >90 modal%) bodies that are hosted in the intermediate igneous rocks of the Punta del Cobre Formation (e.g., diorite, andesite; Pincheira et al., 1990). The ore bodies measure approximately 1500 m long, ~150 m wide, ~500 m deep, and are oriented along strike of the southern portion of the AFS. The West and East ore bodies contain ~63% and ~55% total Fe, respectively, and are bounded on the west by a fault and the east by an Fe-rich brecciated zone (Fe_{total} = ~25%) that extends into dioritic wallrock (Fig. 2). Microscopic observations of samples collected from Los Colorados drill cores and mine pit indicate a lack of sodic and potassic alteration (Knipping et al., 2015b), which makes Los Colorados an ideal natural laboratory to investigate the source of metals in IOA systems.

3. SAMPLE PROCUREMENT AND PREPARATION

3.1. Chilean iron belt samples

Los Colorados drill core samples were acquired in cooperation with the Compañia Minera del Pacifico. In order to study the origin of the iron oxide ore in this deposit, we retrieved samples from two drill cores from the West Ore Body (Fig. 2): (1) core LC-04, which penetrates the northern edge of the West Ore Body and extends into wall rock meta-andesite; (2) core LC-05, which was drilled through the middle portion of the West Ore Body and extends into a brecciated diorite at the base of the ore body. Massive magnetite samples span the entire ~150 m length of each drill core in order to investigate any spatial heterogeneity within the ore deposit. Additional samples were collected from the operating pit area, including one from the East Ore Body. This allowed us to roughly compare the composition of the two magnetite ore bodies. We also collected samples of large (>1 cm) disseminated magnetite crystals from the smaller Mariela IOA deposit of the Atacama Region (Fig. 1), and obtained samples from the Plio-Pleistocene El Laco “magnetite lavas”, which remains one of the most enigmatic Chilean IOA deposits and whose genesis remains controversial (e.g., Henríquez and Nyström, 1998; Rhodes and Oreskes, 1999; Sillitoe and Burrows, 2002; Nyström et al., 2008; Naranjo et al., 2010; Dare et al., 2014). The El Laco samples were collected from a drill core in the Pasos Blancos area, about 1 km south of Pico Laco (Naranjo et al., 2010), and are also massive magnetite.

3.2. Samples from other localities

We also analyzed massive magnetite samples from other well-studied IOA deposits (Table 1). These locations include the Kiruna IOA deposit in northern Sweden and the Mineville IOA deposit in New York, USA (Fig. 1). The Mineville magnetite represented a deposit formed from secondary hydrothermal activity; thus, the Mineville IOA is extensively altered. Disseminated magnetite from the magmatic–hydrothermal Granisle porphyry Cu deposit in British Columbia, CA (Wilson et al., 1980;

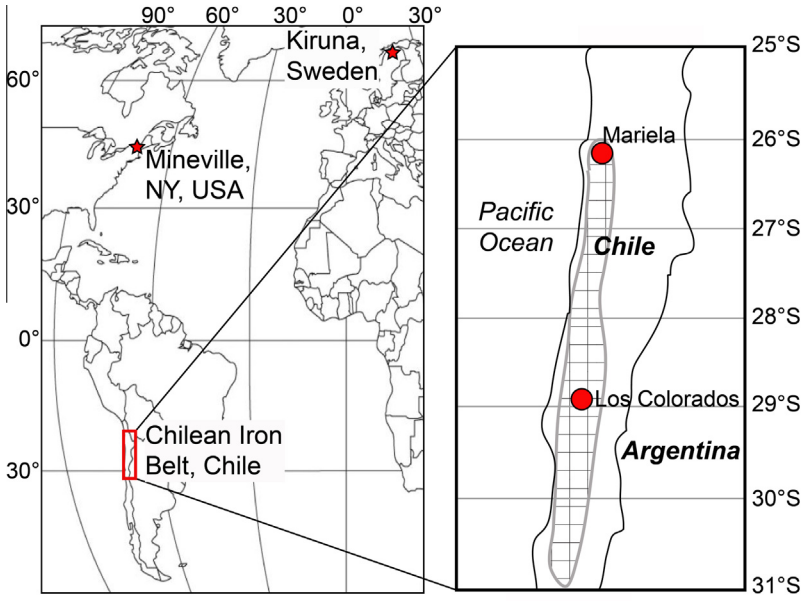

Fig. 1. Map in left panel shows the locations of the three IOA districts focused on by this study. Right panel zooms into the Chilean iron belt (gray hatched area) and the iron oxide-apatite deposits analyzed here. The El Laco deposit is located northeast of the belt at 23°48S.

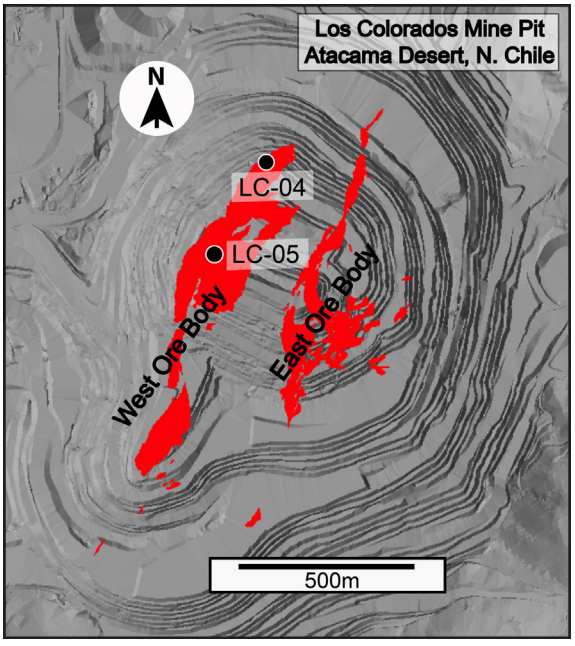

Fig. 2. Map view of the West and East Ore Bodies (red areas) within the pit of the Los Colorados Iron Mine. Circles indicate surface locations of the two drill cores (LC-04 and LC-05) analyzed in this study. (For interpretation of the references to color in this figure legend, the reader is referred to the web version of this article.)

Quan et al., 1987), the Kuna Crest granodiorite of the Tuolumne Intrusive Series (TIS), USA (e.g., Paterson et al., 2008), and the Bushveld Igneous Complex (e.g., VanTongeren et al., 2010) were used as controls of magnetite of a known magmatic origin.

4. ANALYTICAL METHODS

4.1. Sample selection and preparation for analysis

Whole rock samples from the magnetite ore bodies were hand-crushed by using an agate mortar and pestle that was rinsed in ethanol between samples to avoid contamination. Magnetite was separated from the crushed whole rock by using a hand magnet wrapped in a Kimwipe. Grains were then inspected under a microscope at ~40× magnification to ensure that no other mineral phases were present. Thin sections from corresponding samples were also inspected. For all isotopic measurements, only minerals without visible impurities were used. The magnetite was crushed after inspection to a powder with the agate pestle prior to laser fluorination for O isotope analysis and dissolution for Fe isotope analysis. Actinolite was handpicked under a binocular microscope before O isotope analysis to avoid grains with impurities.

4.2. Oxygen isotopes

Oxygen isotope analyses were performed on mineral separates at the University of Oregon by using a laser fluorination line attached to MAT 253 gas isotope ratio mass spectrometer (IRMS) in dual inlet mode, and using BrF_5 as reagent. About 2 mg of magnetite and 1.5 mg of actinolite were used for each analysis. Notably, although samples were carefully handpicked to avoid impurities, the Los Colorados magnetite contains sub-microscopic melt inclusions (Knipping et al., 2015a) that cause them to behave unpredictably during interaction with the laser in the presence of BrF_5; crystals would move around and out of their places in the sample holder. Therefore, later analyses were performed on pressed more finely powdered

Table 1
Iron and O isotope data for magnetite and actinolite mineral separates. NA indicates that samples were not analyzed for that isotope. Los Colorados sample names refer to the drill core and depth within the core where the sample was taken (e.g., 05–3.30 indicates core LC-05, 3.30 m from the top of the drill hole). All magnetite samples are massive magnetite ore except TIS and GR-1, which are disseminated magnetite. Note that depths in this Table differ from those presented in Fig. 2 where the depths correspond to true depth from Earth's surface.

Location	Sample	Phase	δ^{56}Fe (‰)	2σ	δ^{18}O (‰)	2σ
Chilean iron belt						
Los Colorados (LC)						
Core LC-05	05–3.30	Magnetite	0.22	0.03	2.41	0.02
	05–20.7	Magnetite	0.09	0.06	3.04	0.05
	05–32	Magnetite	0.22	0.03	2.75	0.04
	05–52.2	Magnetite	0.14	0.08	3.17	0.03
	05–72.9	Magnetite	0.13	0.05	2.36	0.04
		Actinolite 1	NA	NA	6.18	0.12
		Actinolite 2	NA	NA	6.74	0.12
	05–82.6	Magnetite	0.08	0.03	2.76*	0.10
	05–90	Magnetite	0.21	0.07	2.99	0.10
	05–106	Magnetite	0.12	0.03	2.78	0.03
	05–126.15	Magnetite	0.10	0.06	2.48	0.03
	05–129.3a	Magnetite	0.22	0.05	NA	NA
	05–129.3b	Magnetite	0.14	0.02	NA	NA
Core LC-04	04–38.8	Magnetite	0.18	0.03	2.04	0.03
	04–66.7	Magnetite	0.18	0.07	1.92*	0.08
	04–129.3	Magnetite	0.22	0.03	2.62*	0.04
	04–104.4	Magnetite	0.24	0.08	2.43*	0.58
LC East Ore Body	pitE1	Magnetite	0.18	0.03	NA	NA
El Laco	LCO-39	Magnetite	0.39	0.09	4.00	0.10
	LCO	Magnetite	0.29	0.03	NA	NA
	LCO vein	Magnetite	0.30	0.03	4.34	0.10
	LCO-76	Magnetite	0.32	0.09	NA	NA
	LCO-78	Magnetite	0.53	0.03	NA	NA
	LCO-104	Magnetite	0.27	0.03	NA	NA
	LCO-111	Magnetite	0.20	0.03	NA	NA
Mariela	M-8	Magnetite	0.13	0.03	1.49	0.04
Other IOAs						
Mineville, NY	Mineville	Magnetite	−0.92	0.03	−0.79	0.03
Kiruna, Sweden	KRA-9	Magnetite	0.16	0.03	1.76	0.25
Other igneous						
Tuolumne Intrusive Series (Kuna Crest)	TIS	Magnetite	0.20	0.03	0.88*	0.12
Granisle Porphyry	GR-1	Magnetite	NA	NA	2.70*	0.12

* Samples required a cold finger for O isotope analysis because they yielded between 7.8 and 15 μmol.

samples, exposing the entirety of the sample material to one power level before increasing the laser power in increments of one percent. A cold finger was used for any sample that yielded only 7.8–15 μmol total O_2 (Table 1). In-house Gore Mountain garnet standard (+6.52‰) was used as a standard and was analyzed before sample measurements began, in the middle of the sample queue, and once after all samples. Oxygen isotope values are reported in Table 1 relative to the international standard VSMOW, following Eq. (1):

$$\delta^{18}O_{sample}(‰) = [(^{18}O/^{16}O)_{measured}/(^{18}O/^{16}O)_{VSMOW} - 1] * 1000 \quad (1)$$

The average measured standard values ($\delta^{18}O_{GMGarnet} \pm 1\sigma$) obtained during two days of instrument use were 6.90 ± 0.12‰ and 6.83 ± 0.10‰ and values of the unknowns were adjusted to be on a SMOW scale.

4.3. Iron isotopes

Ion chromatography was performed on all samples to isolate Fe from mineral samples for isotopic analysis. Magnetite samples (<1 mg) were first dissolved and dried down in aqua regia, and then dissolved and dried down again in 8 N HCl, before being loaded into columns with AG1-X8 resin in 8 N HCl, following the procedure of Huang et al. (2011). Only a small amount of magnetite was necessary to have enough detectable Fe and a large amount was avoided so as not to overload the column resin. All acids (HCl, HNO_3) and water used during this process were ultrapure. Samples were analyzed by using a Nu Plasma HR multi-collector inductively coupled plasma mass spectrometer (MC-ICP-MS) in dry plasma mode with a Desolvating Nebuliser System at the University of Illinois, Urbana-Champaign. All analyses were performed following the double-spike method of Millet et al. (2012), in which

a standard solution of $^{57}Fe/^{58}Fe$ was added to each sample to correct for instrumental mass bias and increase precision. International standard IRMM-14 was measured between every sample to monitor and correct for instrumental drift throughout each session (Millet et al., 2012). Iron isotope data are reported in Table 1 relative to IRMM-14, following the relationship of Eq. (2):

$$\delta^{56}Fe_{sample}(‰) = [(^{56}Fe/^{54}Fe)_{measured}/(^{56}Fe/^{54}Fe)_{IRMM-14} - 1] * 1000 \quad (2)$$

Long-term reproducibility of U.S.G.S. rock powder standard BCR-2 was 0.07 ± 0.02‰ (1SE, $n = 14$, 2 sessions over 3 months) and the average standard deviation of sample measurements (2σ) was 0.04‰.

4.4. Hydrogen isotopes and water content of Los Colorados magnetite and actinolite

The stable H isotopic compositions and water contents of magnetite and actinolite were determined by using a thermal conversion elemental analyzer with a MAT253 gas source IRMS at the University of Oregon following the analytical methods of Bindeman et al. (2012). Hydrogen isotope data are reported in Section 5.5 relative to SMOW, following the relationship of Eq. (3):

$$\delta D_{sample}(‰) = [(^{2}H/^{1}H)_{measured}/(^{2}H/^{1}H)_{VSMOW} - 1] * 1000 \quad (3)$$

4.5. Major element analyses of actinolite grains

Major element concentrations of actinolite were measured with Wavelength Dispersive Spectroscopy (WDS) by using a Cameca SX-100 electron probe microanalyzer (EPMA) at the University of Michigan, Ann Arbor, following the method of Lledo and Jenkins (2008). A 15 nA beam was used with an accelerating voltage of 15 kV. We calibrated by using the following standards: ferrosillite (Fe), geikielite (Mg, Ti), tanzanite (Al), orthoclase (Si, K), wollastonite (Ca), rhodonite (Mn), and albite (Na). Sodium and Mg Kα were measured by using the LTAP crystal, TAP was used for Al and Si, PET was used for K and Ca, LPET for Ti, and the LLIF crystal was used to measure Mn and Fe. Counting times were 10 s on peak for all elements.

5. RESULTS

5.1. Mineralogy of the Los Colorados samples

The samples collected from Los Colorados are dominantly (up to 90 modal%) magnetite with an average of 5–10 modal% (combined) actinolite and apatite, and sparse (⩽5 modal%) quartz, clinopyroxene, orthopyroxene, titanite, and calcite. Crystals of quartz and calcite are interpreted to be secondary as they fill veins or cracks in the magnetite drill core samples. Actinolite occurs in some samples at up to 15 modal%, particularly in the pit sample collected from the East Ore Body. The modal abundances remain nearly constant throughout the length of cores LC-04 and LC-05. A representative backscatter electron image of actinolite within magnetite ore (sample 05–82.6) is shown in Fig. 3. Macroscopically and microscopically, actinolite and magnetite crystals have an intergrown texture, which suggests that they grew simultaneously.

5.2. Oxygen isotope compositions of magnetite separates

Stable O isotope values for magnetite separates are reported as $\delta^{18}O$ values in Table 1 and shown in Fig. 4. The average value of $\delta^{18}O$ ($\pm 2\sigma$) of the Los Colorados magnetite sampled from cores LC-04 and LC-05 is 2.32 ± 0.12‰ ($n = 7$) and 2.76 ± 0.12‰ ($n = 11$), respectively (n refers to the number of unique samples from different depths of the core). Magnetite from the Mariela IOA deposit yielded a $\delta^{18}O$ of 1.49 ± 0.04‰, and magnetite from the Mineville IOA deposit yielded a $\delta^{18}O$ value of −0.79 ± 0.03‰. The Kiruna sample has a $\delta^{18}O$ value of 1.76 ± 0.25‰ ($n = 2$), and analyses of two El Laco magnetite samples yielded $\delta^{18}O$ values of 4.00 ± 0.10‰ (LCO-39) and 4.34 ± 0.10‰ (LCO vein) (Table 1). The $\delta^{18}O$ values presented here are consistent with the very limited published O isotope data for IOA and IOCG deposits (e.g., Rhodes and Oreskes, 1999; Nyström et al., 2008; Jonsson et al., 2013). Unequivocally magmatic–hydrothermal magnetite from the Granisle porphyry deposit and the igneous Kuna Crest (TIS) granodiorite yielded $\delta^{18}O$ values of 2.70 ± 0.12‰ and 0.88 ± 0.12‰, respectively.

5.3. Iron isotope composition of magnetite separates

Stable Fe isotope data for magnetite separates are reported in Table 1 and Fig. 4. Los Colorados core LC-04 magnetite $\delta^{56}Fe$ ($\pm 2\sigma$) values range from 0.18 ± 0.03‰ to 0.26 ± 0.04‰ ($\delta^{56}Fe_{average} = 0.20‰$; $n = 8$) and core LC-05 magnetite $\delta^{56}Fe$ values range from 0.08 ± 0.08‰ to 0.22 ± 0.05‰ ($\delta^{56}Fe_{average} = 0.15‰$; $n = 9$). Magnetite from pit samples of the East Ore Body yielded a $\delta^{56}Fe$ of 0.24 ± 0.02‰. The data for samples from both

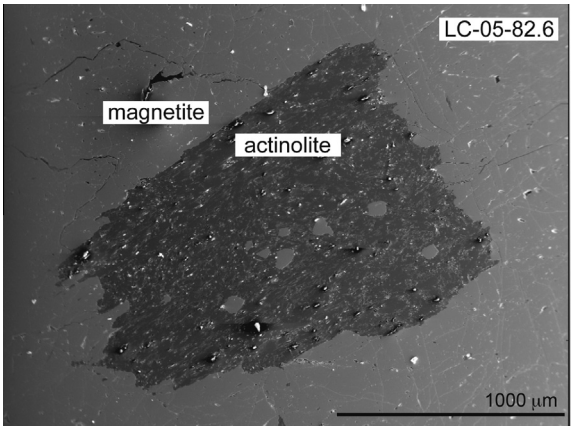

Fig. 3. Backscatter electron image of a representative actinolite grain intergrown with magnetite from Los Colorados core LC-05, depth 82.6 m. The phase both surrounding and within the actinolite grain is magnetite.

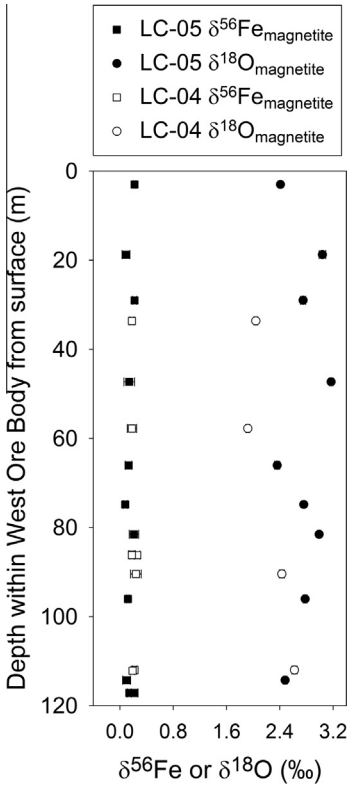

Fig. 4. All Los Colorados stable Fe and O isotope data plotted for both core LC-05 and LC-04 within the West Ore Body. The drill cores were not vertical. True depth from Earth's surface was calculated for each sample according to the dip and length of each drill core (data provided by Compañia Minera del Pacifico). Error bars for all data are 2σ.

of the Los Colorados West Ore Body drill cores are stratigraphically homogeneous within the ore sampled by the drill core (Fig. 4).

The δ^{56}Fe composition of magnetite from the Mariela IOA deposit is 0.13 ± 0.03‰ and 0.57 ± 0.04‰, respectively, and Mineville magnetite yielded a δ^{56}Fe value of -0.92 ± 0.03‰. Kiruna magnetite has a δ^{56}Fe of 0.16 ± 0.07‰. Magnetite from El Laco ranges from $\delta^{56}Fe = 0.20 \pm 0.03$‰ to 0.53 ± 0.03‰ ($\delta^{56}Fe_{average} = 0.33$‰; $n = 7$). Magnetite Fe isotope compositions have also been measured in samples of the Upper and Upper Main Zone of the Bushveld Complex, South Africa, previously characterized by VanTongeren et al. (2010), VanTongeren and Mathez (2012), Bilenker et al. (2014). The δ^{56}Fe values obtained from these samples range from 0.28 ± 0.04‰ to 0.86 ± 0.07‰. The Kuna Crest granodiorite contained magnetite with an Fe isotope composition of $\delta^{56}Fe = 0.20 \pm 0.03$.

5.4. Oxygen isotope composition and Fe number of actinolite

Actinolite from Los Colorados sample 05–72.9 yielded a δ^{18}O value of 6.46 ± 0.56‰. The Fe number (Fe # = [molar Fe]/[molar Fe + molar Mg]; c.f. Lledo and Jenkins, 2008) of actinolite was calculated for individual actinolite grains sampled from core LC-05 (depth = 82.6 m; sample name 05–82.6), one pit sample from the West Ore Body (pitW3), and one pit sample from the East Ore Body (pitE1). The average Fe # ($\pm 1\sigma$) for all grains measured in each of these samples is 0.44 ± 0.11 ($n = 8$), 0.35 ± 0.05 ($n = 16$), and 0.52 ± 0.02 ($n = 8$), respectively. All analytical data for actinolite are reported in Table 2.

5.5. Hydrogen isotopes and water content of Los Colorados magnetite and actinolite

Los Colorados actinolite contains 2.08 ± 0.04 wt% water, while magnetite grains contained 0.10 ± 0.07 wt% water. The large error on the magnetite water content is due to the small amount of water present in the sample. The stable H isotope composition of the actinolite was $\delta D = -59.3 \pm 1.7$‰ while magnetite grains had δD value of -53.5 ± 1.5‰.

6. DISCUSSION

6.1. Constraints on the source of Fe and O in IOA deposits

Traditionally, O and H stable isotope ratios have been used to establish "boxes", or ranges, of the isotopic composition of rocks and minerals formed from specific processes, such as precipitation from a meteoric fluid versus precipitation from a magmatic–hydrothermal fluid exsolved directly from a silicate melt (e.g., Hedenquist and Lowenstern, 1994). However, since Fe-rich ore deposits occasionally lack abundant H-bearing phases, and may contain only H-bearing minerals that are paragenetically post-mineralization, developing source ranges for stable Fe–O isotope pairs offers the opportunity to fingerprint directly the source of Fe and O in IOAs.

The global range of O isotope values for igneous magnetite (i.e., magnetite crystallized directly from silicate melt) was constrained by Taylor (1967, 1968) as $\delta^{18}O = 1.0$–4.4‰. Bindeman and Valley (2002, 2003) present precise laser fluorination analyses of coexisting quartz and magnetite from a variety of major silicic ignimbrites around the world and the stable O isotope compositions of the magnetite grains range from +1.5 to +4.5‰.

Similarly, for stable Fe isotopes, Heimann et al. (2008) and Weis (2013) reported a global range for igneous magnetite of $\delta^{56}Fe = 0.06$–0.49‰. In these studies, igneous magnetite was sampled from plutonic and volcanic rocks across silica contents, and the values represent those of unaltered, primary igneous magnetite.

The method of using Fe and O isotope ratios for source fingerprinting was first employed successfully on IOA samples by Weis (2013) who focused on the >1.85 Ga Grängesberg Mining District (GMD), Sweden. Iron isotope data are useful because Fe is abundant in the deposit, exists within the mineral of economic interest, and the Fe isotope compositions of minerals appear to be less affected by secondary processes than other isotopic systems. Weis (2013) demonstrated this by quantifying the Fe and O isotope values of magnetite grains within and around the GMD ore deposit as well as samples from other Fe-rich deposits of

Table 2
Fe and Mg concentrations and calculated Fe # of actinolite grains in the Los Colorados magnetite ore bodies. Grain compositions were obtained by point or line traverse EPMA measurements; averages of the values of the latter were used for the grains with an asterisk. Temperature (T) values were obtained by using the approach of Lledo and Jenkins (2008).

Location	Grain ID	Mg (molar)	Fe (molar)	Fe # (grain average)	Estimated T (°C) at 100; 200 MPa
pit west	1	3.36	1.98	0.37	745; 780
pit west	2	3.34	2.02	0.38	740; 765
pit west	3*	3.33	2.13	0.39	730; 760
pit west	4	3.39	1.58	0.32	760; 790
pit west	5	3.41	1.66	0.33	755; 785
pit west	6	3.33	1.84	0.36	750; 780
pit west	7	3.26	2.40	0.42	705; 740
pit west	8*	3.32	2.18	0.40	725; 755
pit west	9	3.44	1.66	0.32	760; 790
pit west	10	3.12	2.42	0.44	710; 740
pit west	11	3.25	1.65	0.34	750; 780
pit west	12	3.39	1.61	0.32	760; 790
pit west	13*	3.34	2.06	0.38	740; 765
pit west	14*	3.32	2.15	0.39	730; 760
pit west	15	3.63	1.10	0.23	780; 810
pit west	16	3.61	1.17	0.25	785; 805
			Average:	0.35	750; 780
pit east	1*	2.92	3.41	0.54	670; 690
pit east	2*	2.94	3.33	0.53	680; 700
pit east	3*	2.80	3.33	0.54	670; 690
pit east	4	2.89	3.24	0.53	680; 700
pit east	5	2.87	3.32	0.54	670; 690
pit east	6	2.96	3.42	0.54	670; 690
pit east	7	3.03	3.03	0.50	690; 715
pit east	8	3.08	2.86	0.48	695; 725
			Average:	0.52	680; 700
core 5 82.6	1	3.25	2.09	0.38	740; 765
core 5 82.6	2	1.99	5.14	0.72	620; 640
core 5 82.6	3	3.32	1.95	0.37	745; 770
core 5 82.6	4	3.40	2.66	0.38	740; 765
core 5 82.6	5*	3.34	1.60	0.40	725; 755
core 5 82.6	6*	3.10	2.44	0.43	710; 740
core 5 82.6	7	3.18	2.66	0.46	700; 725
core 5 82.6	8	3.24	2.22	0.41	715; 740
			Average:	0.44	710; 740
Los Colorados			Average:	0.44	710; 740
			2σ	0.28	

* Denotes average values of EPMA line traverse rather than a point measurement.

known igneous origin (e.g., basalt, basaltic andesite, dacite, dolerite). The Fe isotope data showed less variation and plotted within the known igneous range (cf. Heimann et al., 2008), while the O isotope compositions of some of the magnetite samples plot outside of the range interpreted to represent igneous O isotope values (c.f. Taylor, 1967; 1968) (Fig. 5, white circles).

All published Fe–O isotope pairs (Weis, 2013; this study) are plotted in Fig. 5 along with the accepted bounds of the magmatic Fe–O isotope box. The Los Colorados and other CIB samples (El Laco, Mariela) plot distinctively within the range of magmatic values along with Kiruna magnetite and one of our examples of an unequivocally magmatic deposit, the Granisle porphyry. Fluid inclusion analyses indicate temperatures of 400–700 °C for the potassic alteration and ore formation at Granisle (Wilson et al., 1980; Quan et al., 1987).

The consistency of these Fe–O pairs with the established magmatic box suggests a high-temperature origin for these IOA deposits. Since the few available Fe–O isotope pairs are not limited to Chilean and Swedish IOA deposits, we can begin to identify areas beyond the magmatic box where samples formed due to other processes. However, additional data are needed to refine these other potential boxes. For example, magnetite from the pervasively altered Mineville IOA deposit has particularly low δ^{56}Fe and δ^{18}O compositions. By combining field relations, geochronology, and geochemical compositions of host, mineralized, and later-emplaced rocks, Valley et al. (2011) concluded that secondary fluids remobilized magmatic magnetite to form new Fe-oxide deposits at Mineville. Since it has been shown by theoretical calculations and experimental data that Cl-bearing fluids preferentially incorporate ^{54}Fe relative to magnetite (e.g., Heimann et al., 2008; Hill and Schauble,

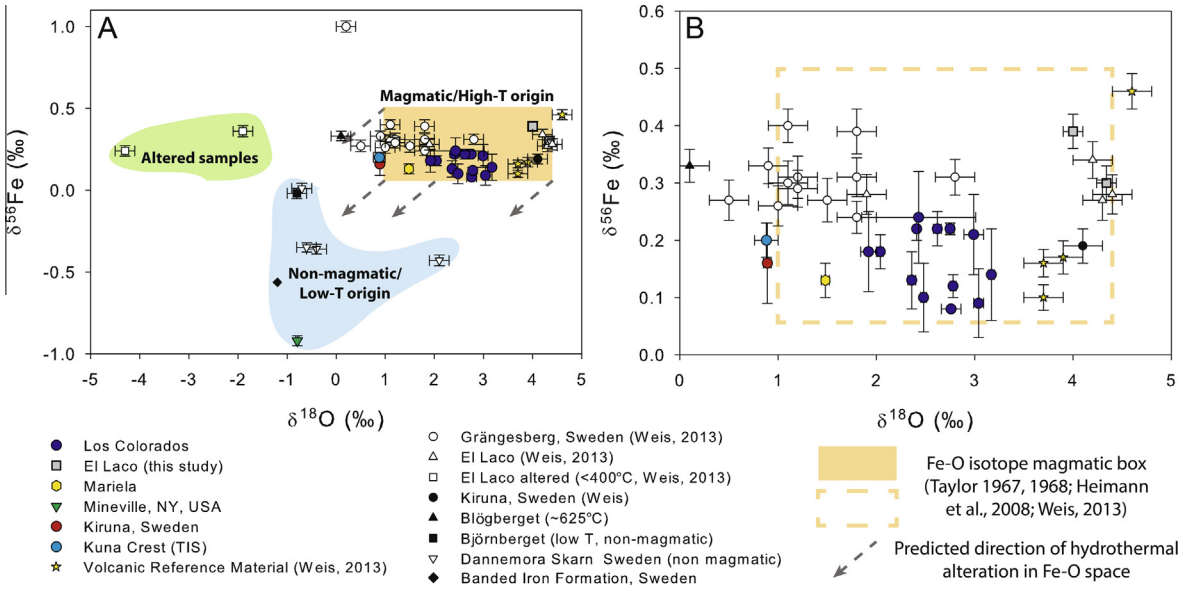

Fig. 5. Isotopic data for magnetite samples in δ^{56}Fe vs. δ^{18}O space. Colored symbols represent samples measured in this study, and white or black symbols represent data reported by Weis (2013). The solid and dashed orange boxes denote magmatic isotope ranges as established by Taylor (1967, 1968), Heimann et al. (2008), and Weis (2013). Yellow stars denote Fe and O isotope values for igneous magnetite reported by Weis (2013). Panel A displays all data discussed while panel B show only datasets that include samples plotting within the magmatic Fe–O box. All Los Colorados samples have magmatic Fe–O isotope values. Error bars are 2σ. (For interpretation of the references to colour in this figure legend, the reader is referred to the web version of this article.)

2008; Bilenker et al., 2013; Bilenker, 2015), our Fe–O isotope data agree with the hypothesis of Valley et al. (2011). The other samples with lighter Fe–O isotope compositions than the magmatic box are from the Dannemora Iron skarn deposit, Sweden (Weis, 2013; Fig. 5, white circles). This skarn was formed by contact metamorphism when a magma body intruded carbonate wall rocks (Lager, 2001). The Fe–O isotope data are close to but outside of the magmatic ranges, consistent with the interaction of magmatic fluids and sedimentary rocks that formed from isotopically lighter, lower-temperature fluids.

Our El Laco data are consistent with the previously published values of δ^{18}O reported by Rhodes and Oreskes (1999), Nyström et al. (2008). However, while the magnetite data reported by Rhodes and Oreskes (1999) fit within the range for igneous magnetite, they were interpreted by the authors of that study to indicate precipitation of magnetite from isotopically heavy non-magmatic fluids, hypothesized to have been derived from interaction with an evaporitic source. These conclusions were based upon the fact that "hydrothermal" and "magmatic" magnetite at El Laco have similar O isotope values. Nyström et al. (2008) used their O isotope data to complement field observations and fluid inclusion data and concluded that the El Laco magnetite has a magmatic origin with minimal secondary alteration from interaction with low-temperature, post-formation fluids. Since we now also have constraints for magmatic Fe isotopes, our Fe–O isotope pairs are consistent with the latter hypothesis and seem to demand a magmatic or magmatic–hydrothermal formation for El Laco. Importantly, the Fe isotope data obtained from the Bushveld provide another source of unequivocally magmatic magnetite, and plot within and above the δ^{56}Fe range as determined by Heimann et al. (2008) and Weis (2013). Therefore, we can use these new data to extend the δ^{56}Fe range of the magmatic magnetite Fe–O box to 0.06–0.86‰ (Fig. 6). Lastly, the certainly magmatic magnetite of Kuna Crest had an O isotope composition slightly lower than the established magmatic range ($\delta^{18}O = 0.88 \pm 0.12$‰), but its error brings the δ^{18}O value to overlap with the established range.

It is also worthy to note that the Weis (2013) Kiruna datum matches our new Kiruna sample in Fe isotope value, but not in O isotope value. Since "Kiruna" encompasses a suite of deposits in Sweden, it is possible that the discrepancy in δ^{18}O value reflects disturbance from fluid interactions with this very old deposit. This is consistent with what Weis (2013) demonstrated in determining that the Fe isotope composition of magnetite would be less affected by post-formation fluid-interaction. This is further evinced in Fig. 5, where altered El Laco samples (green area) retain similar Fe isotope signatures as the other El Laco samples while shifting to lighter O isotope compositions as fluids tend to preferentially incorporate lighter isotopes. Additionally, the blue region outlines samples that were formed by non-magmatic, low-temperature processes. Neither the Fe nor O isotope values are consistent with the range that establishes the "magmatic box."

6.2. Hydrogen isotope constraints on magnetite and actinolite source

Our stable H isotope data also corroborate a high-temperature and non-meteoric source. The δD values are consistent with each other (−53.5‰ magnetite versus −59.4‰ actinolite), suggesting growth in the presence the

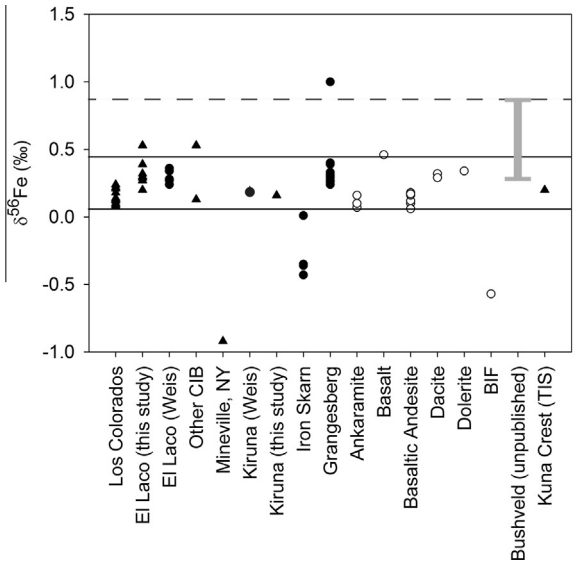

Fig. 6. Iron isotope compositions of magnetite measured in this study (triangles) and data reported by Weis (2013) (circles). The open circles highlight data for unaltered igneous magnetite ("Volcanic Reference Material" from New Zealand, the Canary Islands, Iceland, Indonesia, Cyprus). The vertical gray bar for the Bushveld represents the range of δ^{56}Fe values obtained from magnetite separates. Solid horizontal lines indicate the upper and lower δ^{56}Fe values reported by Heimann et al. (2008) for magnetite from unaltered volcanic and plutonic rocks. The horizontal dashed line is the upper δ^{56}Fe values when igneous magnetite from the Bushveld intrusion is included.

same fluid or fluids of the same origin. In particular, these values indicate a mantle source of H (Craig and Lupton, 1976). When paired with their respective O isotope values, the data are consistent with a non-meteoric origin (c.f Hedenquist and Lowenstern, 1994).

6.3. Constraints on the minimum formation temperature of Los Colorados

6.3.1. Isotopic constraints

We calculated minimum formation temperatures by using the difference in O isotope composition between magnetite and actinolite by using Eq. (4) (cf. Bindeman and Valley, 2002):

$$\Delta^{18}O_{\text{actinolite-magnetite}} = \delta^{18}O_{\text{actinolite}} - \delta^{18}O_{\text{magnetite}} \sim 1000 \ln \alpha \quad (4)$$

The $\Delta^{18}O_{\text{actinolite-magnetite}}$ of the actinolite-magnetite pair analyzed from sample 05–72.9 is 4.10‰ ($\delta^{18}O_{\text{actinolite}} - \delta^{18}O_{\text{magnetite}} = 6.46‰ - 2.36‰$). By using the measured $\Delta^{18}O_{\text{actinolite-magnetite}}$, the minimum formation temperature can be calculated via Eq. (5):

$$1000 \ln \alpha = 10^6 A / T^2 \quad (5)$$

where A is the experimentally-determined A factor for the linear relationship between O isotope fractionation between magnetite and amphibole and $10^6/T^2$ through 0 ($A = 3.36$ here); T is temperature in Kelvin. If we use an A factor of 3.36 for clinopyroxene as a proxy for actinolite (Chiba et al., 1989), then the calculated minimum temperature of formation is ~630 °C, consistent with the closure temperature of magmatic magnetite for O isotopes (e.g., Farquhar et al., 1993; Farquhar and Chacko, 1994; Huaiwei, 2014).

We also used published fractionation factors to calculate the isotopic composition of the hypothetical parent magma and magmatic water that may have formed Los Colorados. We used data for an andesite, a composition commonly associated with the formation of IOAs: $\Delta^{18}O_{\text{magnetite-andesite}} = -4.0‰$, $\Delta^{18}O_{\text{magnetite-water}} = -4.5‰$ (Zhao and Zheng, 2003). Using Eq. (4) and the average δ^{18}O of Los Colorados magnetite (2.60 ± 0.74‰), the isotopic compositions of the parent magma and co-existing magmatic water are calculated to be 6.60‰ and 7.10‰, respectively. This is consistent with the O isotope composition of subduction zone magmas, such as those associated with the formation of IOA deposits (Taylor, 1968; Bindeman, 2008; Jonsson et al., 2013).

6.3.2. Geochemical constraints

The Fe # values calculated for actinolite from the Los Colorados deposit are consistent with high-temperature growth of actinolite (Table 2). We compared these Fe # values to the experimental data of Lledo and Jenkins (2008) to obtain a reasonable estimation of the formation temperature of actinolite at a pressure range consistent with the estimated depths of formation for Los Colorados (100–200 MPa). The average Fe # of 0.44 for all Los Colorados actinolite samples yields calculated formation temperatures that range from 710 to 740 °C at 100 and 200 MPa, respectively. Applying the highest (Fe # = 0.72) and lowest (Fe # = 0.23) Fe # to the temperature ranges corresponding with pressures of 100 and 200 MPa yields a minimum temperature of 620 °C and a maximum temperature of 810 °C. These temperatures are consistent with the closure temperatures calculated from actinolite-magnetite O isotope values, as well as previous studies on similar deposits (El Laco, Nyström et al., 2008; Grängesburg, Weis, 2013).

6.4. Implications for the formation of iron oxide-apatite deposits

The Fe and O stable isotope compositions of magnetite, combined with the O isotope composition and Fe # of syngenetic actinolite, and the H isotope compositions of actinolite and magnetite reported here demonstrate that both Fe and O in magnetite from the Chilean Fe oxide deposits (Los Colorados, El Laco, Mariela) and the Kiruna IOA deposit were sourced from a magmatic reservoir (Fig. 5). We invoke high-temperature processes to form IOA deposits, however, these geochemical methods alone do not reveal whether purely magmatic (e.g., crystallization from a magma, liquid immiscibility) or magmatic–hydrothermal processes are responsible. These data are consistent with Weis (2013) and in agreement with the model proposed by Knipping et al. (2015a) supporting a magmatic/magmatic–hydrothermal origin for Los Colorados and other IOA deposits. Additionally for Los Colorados, Knipping et al. (2015b) also found high Ti, V, Al, Mn, and Ga

concentrations in the massive magnetite that are inconsistent with crystallization from surface basinal brines. In addition, melt inclusions re-homogenized as part of this study indicate trapping temperatures above 950 °C. Further development of this method by using additional geochemical data to study a wide variety of global samples will allow it to become a robust, independent geochemical tool.

7. CONCLUSIONS

We report stable Fe and O isotope ratios for magnetite from several iron oxide–apatite (IOA) ore deposits, and combine these data with Fe and O isotope ratios from unequivocally magmatic and magmatic–hydrothermal magnetite to elucidate the source reservoir for these elements in these deposits. The $\delta^{18}O$ and $\delta^{56}Fe$ values for all samples cluster in the ranges 1.0–4.4‰ and 0.06–0.86‰, respectively. These Fe and O isotope data demonstrate that Fe and O in magnetite in IOA deposits are sourced from a magmatic reservoir. Pairing stable Fe and O isotope data from magnetite is a promising new method for fingerprinting the source of these elements in magnetite-bearing ore deposits. Further, we combine Fe and O isotope ratio data for magnetite and actinolite as well as the Fe # of actinolite grains from the world-class Los Colorados IOA deposit, Chile, to conclude that this deposit formed by high-temperature processes. At present, Fe and O isotope pairs do not allow us to discriminate whether magnetite crystallized from a melt or precipitated from a high-temperature magmatic–hydrothermal fluid, but future refinement of the Fe–O isotope source boxes may eventually allow this distinction.

ACKNOWLEDGEMENTS

The authors would like to express gratitude to F. Weis and three anonymous reviewers for valuable feedback that greatly improved the paper. This project was made possible by funding to LDB from the Society of Economic Geologists and UM Department of Earth & Environmental Sciences as well as NSF EAR 1264537, NSF EAR 1264560, and NSF EAR 1250239 to ACS. FB and MR acknowledge funding from Fondecyt grant 1140780, funding from Millennium Science Initiative grant "Nucleaus for Metal Tracing Along Subduction" (NC130065), and FONDAP grant 15090013. We thank Compañia Minera del Pacifico and mine geologist Mario Lagos for logistical assistance.

REFERENCES

Barton M. D. (2014) Iron Oxide(-Cu-Au-REE-P-Ag-U-Co) Systems. In *Treatise on Geochemistry*, second ed., vol. 11, p. 515–541.

Barton M. D. and Johnson D. A. (1996) Evaporitic-source model for igneous-related Fe oxide-(REE-Cu-Au-U) mineralization. *Geology* **24**, 259–262.

Bilenker L. D. (2015) Elucidating Igneous and Ore-Forming Processes by using Fe Isotopes through Experimental and Field-Based Methods. Ph. D. thesis, Univ. of Michigan.

Bilenker L. D., Simon A., Lundstrom C. C., Gajos N. and Zajacz Z. (2013) Experimental constraints on Fe isotope fractionation in fluid-melt-oxide-sulfide assemblages. Goldschmidt Conference.

Bilenker L. D., VanTongeren J. A., Lundstrom C. and Simon A. (2014) Fe isotope systematics of the Upper and Upper Main Zones of the Bushveld Complex, South Africa. AGU Fall Meeting [abs]: V51C–4797.

Bindeman I. (2008) Oxygen isotopes in mantle and crustal magmas as revealed by single crystal analysis. *RiMG* **69**, 445–478.

Bindeman I. N. and Valley J. W. (2002) Oxygen isotope study of the long Valley-Glass Mountain magmatic system, California: isotope thermometry, and t convection in large silicic magma bodies. *Contrib. Mineral. Petrol.* **144**, 185–205.

Bindeman I. N. and Valley J. W. (2003) Rapid generation of both high- and low-$\delta^{18}O$, large volume silicic magmas at Timber Mountain/Oasis Valley caldera complex, Nevada. *Bull. Geol. Soc. Am.* **115**, 581–595.

Bindeman I. N., Kamenetsky V. S., Palandri J. and Vennemann T. (2012) Hydrogen and oxygen isotope behaviors during variable degrees of upper mantle melting: example from the basaltic glasses from Macquarie Island. *Chem. Geol.* **310–311**, 126–136.

Chen H., Cooke D. R. and Baker M. J. (2013) Mesozoic iron oxide copper-gold mineralization in the central andes and the Gondwana supercontinent breakup. *Econ. Geol.* **108**, 37–44.

Chiba H., Chacko T., Clayton R. N. and Goldsmith J. R. (1989) Oxygen isotope fractionations involving diopside, forsterite, magnetite, and calcite: application to geothermometry. *Geochim. Cosmochim. Acta* **53**, 2985–2995.

Craig H. and Lupton J. E. (1976) Primordial neon, helium, and hydrogen in oceanic basalts. *EPSL* **31**, 369–385.

Dare S. A. S., Barnes S.-J. and Beaudoin G. (2014) Did the massive magnetite "lava flows" of El Laco (Chile) form by magmatic or hydrothermal processes? New constraints from magnetite composition by LA-ICP-MS. *Mineral. Dep.*. http://dx.doi.org/10.1007/s00126-014-0560-1.

Farquhar J. and Chacko T. (1994) Exsolution-enhanced oxygen exchange: implications for oxygen isotope closure temperatures in minerals. *Geology* **22**, 751–754.

Farquhar J., Chacko T. and Frost B. R. (1993) Strategies for high-temperature oxygen isotope thermometry: a worked example from the Laramie Anorthosite Complex, Wyoming, USA. *EPSL* **117**, 407–422.

Groves D. I., Bierlein F. P., Meinert L. D. and Hitzman M. W. (2010) Iron Oxide Copper-Gold (IOCG) deposits through earth history: implications for origin, lithospheric setting, and distinction from other epigenetic iron oxide deposits. *Econ. Geol.* **105**, 641–654.

Hedenquist J. W. and Lowenstern J. B. (1994) The role of magmas in the formation of hydrothermal ore deposits. *Nature* **370**, 519–527.

Heimann A., Beard B. L. and Johnson C. M. (2008) The role of volatile exsolution and sub-solidus fluid/rock interactions in producing high $^{56}Fe/^{54}Fe$ ratios in siliceous igneous rocks. *Geochim. Cosmochim. Acta* **72**, 4379–4396.

Henríquez F. and Nyström J. O. (1998) Magnetite bombs at El Laco volcano, Chile. *GFF* **120**, 269–271.

Hill P. S. and Schauble E. A. (2008) Modeling the effects of bond environment on equilibrium iron isotope fractionation in ferric aquo-chloro complexes. *Geochim. Cosmochim. Acta* **72**, 1938–1958.

Hitzman M. W., Oreskes N. and Einaudi M. T. (1992) Geological characteristics and tectonic setting of Proterozoic iron oxide (Cu-U-Au-REE) deposits. *Precambrian Res.* **58**, 241–287.

Huaiwei N. I. (2014) The relationship between apparent equilibrium temperature and closure temperature with application to oxygen isotope geospeedometry. *Chn. J. Geochem.* **33**, 125–130.

Huang F., Zhang Z., Lundstrom C. C. and Zhi X. (2011) Iron and magnesium isotopic compositions of periodotite xenoliths from Eastern China. *Geochim. Cosmochim. Acta* **75**, 3318–3334.

Jonsson E., Troll V. R., Högdahl K., Harris C., Weis F., Nilsson K. P. and Skelton A. (2013) Magmatic origin of giant 'Kiruna-type' apatite-iron-oxide ores in Central Sweden. *Nat. Sci. Rep*. http://dx.doi.org/10.1038/srep01644.

Knipping J. L., Bilenker L. D., Simon A. C., Reich M., Barra F., Deditius A. P., Lundstrom C., Bindeman I. and Munizaga R. (2015a) Giant Kiruna-type deposits form by efficient flotation of magmatic magnetite suspensions. *Geology* **43**, 655–656.

Knipping J. L., Bilenker L. D., Simon A. C., Reich M., Barra F., Deditius A. P., Wälle M., Heinrich C. A., Holtz F. and Munizaga R. (2015b) Trace elements in magnetite from massive iron oxide-apatite deposits indicate a combined formation by igneous and magmatic-hydrothermal processes. *Geochim. Cosmochim. Acta* **171**, 15–38.

Kolker A. (1982) Mineralogy and geochemistry of Fe-Ti oxide and apatite (Nelsonite) deposits and evaluation of the liquid immiscibility hypothesis. *Econ. Geol.* **72**, 1146–1158.

Lager I. (2001) The geology of the Palaeoproterozoic limestone-hosted Dannemora iron deposit, Sweden. Sveriges Geologiska Undersökning Rapporter och meddelanden 107, 49 p.

Lledo H. L. and Jenkins D. M. (2008) Experimental investigation of the upper thermal stability of Mg-rich actinolite implications for Kiruna-type iron deposits. *J. Petrol.* **49**, 225–238.

Lundberg B. and Smellie J. A. T. (1979) Painirova and Mertainen iron ores: two deposits of the Kiruna iron ore type in Northern Sweden. *Econ. Geol.* **74**, 1131–1152.

Mathur R., Marschik R., Ruiz J., Munizaga F., Leveille R. A. and Martin W. (2002) Age of mineralization of the Candelaria Fe oxide Cu-Au deposit and the origin of the Chilean Iron Blet, based on Re-Os isotopes. *Econ. Geol.* **97**, 59–71.

Millet M.-A., Baker J. A. and Payne C. E. (2012) Ultra-precise stable Fe isotope measurements by high resolution multiple-collector inductively coupled plasma mass spectrometry with a ^{57}Fe-^{58}Fe double spike. *Chem. Geol.* **304–305**, 18–25.

Naranjo J. A., Henriquez F. and Nyström J. O. (2010) Subvolcanic contact metasomatism at El Laco Volcanic complex, Central Andes. *Andean Geol.* **37**, 110–120.

Naslund H. R., Henriquez F., Nyström J. O., Vivallo W. and Dobbs F. M. (2002) Magmatic iron ores and associated mineralisation: examples from the Chilean high Andes and coastal Cordillera. In *Hydrothermal Iron Oxide Copper-Gold and Related Deposits: A Global Perspective*: *Adelaide, Australia* (ed. T. M. Porter). PGC Publishing, 2, pp. 207–226.

Nyström J. O. and Henriquez F. (1994) Magmatic features of iron ores of the Kiruna Type in Chile and Sweden: ore textures and magnetite geochemistry. *Econ. Geol.* **89**, 820–839.

Nyström J. O., Billström K., Henríquez F., Fallick A. E. and Naslund H. R. (2008) Oxygen isotope composition of magnetite in iron ores of the Kiruna type in Chile and Sweden. *GFF* **130**, 177–188.

Oyarzun R., Oyarún J., Meénard J. J. and Lillo J. (2003) The Cretaceous iron belt of northern Chile: role of oceanic plates, a superplume event, and a major shear zone. *Mineral. Dep.* **38**, 640–646.

Paràk T. (1975) Kiruna iron ores are not "intrusive-magmatic ores of the Kiruna type". *Econ. Geol.* **70**, 1242–1258.

Paràk T. (1984) On the magmatic origin of iron ores of the Kiruna type: a discussion. *Econ. Geol.* **79**, 1945–1949.

Paterson S. R., Žák J. and Janoušek V. (2008) Growth of complex sheeted zones during recycling of older magmatic units into younger: Sawmill Canyon area, Tuolumne batholith, Sierra Nevada, California. *J. Volc. Geotherm. Res.* **177**, 457–484.

Pincheira M. J., Theile R. and Fontbote L. (1990) Tectonic transpression along the southern segment of the Atacama Fault-Zone, Chile. In Colloques et Seminaires: Symposium International de Geodynamique Andine, Grenoble. pp. 133–136.

Pollard P. J. (2006) An intrusion-related origin for Cu-Au mineralization in iron oxide-copper-gold (IOCG) provinces. *Mineral. Dep.* **41**, 179–187.

Quan R. A., Cloke P. L. and Kesler S. E. (1987) Chemical analyses of halite trend inclusions from the Granisle porphyry copper deposit, British Columbia. *Econ. Geol.* **82**, 1912–1930.

Rhodes A. L. and Oreskes N. (1999) Oxygen isotope composition of magnetite deposits at El Laco, Chile: evidence of formation from isotopically heavy fluids. In *Geology and ore deposits of the Central Andes* (ed. B. J. Skinner). SEG Special Publication 7, 333–351.

Richards J. P. and Mumin A. H. (2013) Magmatic-hydrothermal processes within an evolving Earth: iron oxide-copper-gold and porphyry Cu ± Mo ± Au deposits. *Geology*. http://dx.doi.org/10.1130/G34275.1.

Sillitoe R. H. (2003) Iron oxide-copper-gold deposits: an Andean view. *Mineral. Dep.* **38**, 787–821.

Sillitoe R. H. and Burrows D. R. (2002) New field evidence bearing on the origin of the El Laco magnetite deposit, Northern Chile. *Econ. Geol.* **97**, 1101–1109.

Taylor H. P. (1967) Oxygen isotope studies of hydrothermal mineral deposits. In *Geochemistry of Hydrothermal Ore Deposit, first ed.* (ed. H. L. Barnes). New York, Holt, Rinehart and Winston, pp. 109–142.

Taylor H. P. (1968) The oxygen isotope geochemistry of igneous rocks. *Contrib. Mineral. Petrol.* **19**, 1–71.

Valley P. M., Hanchar J. M. and Whitehouse M. J. (2011) New insights on the evolution of the Lyon Mountain Granite and associated Kiruna-type magnetite-apatite deposits, Adirondack Mountains, New York State. *Geosphere* **7**, 357–389.

VanTongeren J. A. and Mathez E. A. (2012) Large-scale liquid immiscibility at the top of the Bushveld Complex. *Geology* **40**, 491–494.

VanTongeren J. A., Mathez E. A. and Kelemen P. B. (2010) A Felsic End to Bushveld differentiation. *J. Petrol.* **51**, 1891–1942.

Weis F. (2013) Oxygen and Iron Isotope Systematics of the Grängesberg Mining District (GMD), Central Sweden. M. S. thesis, Uppsala universitet.

Wilson J. W. J., Kesler S. E., Cloke P. L. and Kelly W. C. (1980) Fluid inclusion geochemistry of the Granisle and Bell porphyry copper deposits, British Columbia. *Econ. Geol.* **75**, 45–61.

Zhao Z. and Zheng Y. (2003) Calculation of oxygen isotope fractionation in magmatic rocks. *Chem. Geol.* **193**, 59–80.

Associate editor: Edward M. Ripley